Journal of Computational Physics 302 (2015) 222–238

Contents lists available at ScienceDirect

Journal of Computational Physics

www.elsevier.com/locate/jcp

An asymptotic preserving unified gas kinetic scheme for frequency-dependent radiative transfer equations

Wenjun Sun [a], Song Jiang [a], Kun Xu [b,*], Shu Li [a]

[a] Institute of Applied Physics and Computational Mathematics, P.O. Box 8009, Beijing 100088, China
[b] Department of Mathematics and Department of Mechanical and Aerospace Engineering, Hong Kong University of Science and Technology, Hong Kong, China

ARTICLE INFO

Article history:
Received 19 April 2015
Received in revised form 12 August 2015
Accepted 1 September 2015
Available online 11 September 2015

Keywords:
Frequency-dependent radiative transfer
Optically thick and thin
Asymptotic preserving scheme
Unified gas kinetic scheme

ABSTRACT

This paper presents an extension of previous work (Sun et al., 2015 [22]) of the unified gas kinetic scheme (UGKS) for the gray radiative transfer equations to the frequency-dependent (multi-group) radiative transfer system. Different from the gray radiative transfer equations, where the optical opacity is only a function of local material temperature, the simulation of frequency-dependent radiative transfer is associated with additional difficulties from the frequency-dependent opacity. For the multiple frequency radiation, the opacity depends on both the spatial location and the frequency. For example, the opacity is typically a decreasing function of frequency. At the same spatial region the transport physics can be optically thick for the low frequency photons, and optically thin for high frequency ones. Therefore, the optical thickness is not a simple function of space location. In this paper, the UGKS for frequency-dependent radiative system is developed. The UGKS is a finite volume method and the transport physics is modeled according to the ratio of the cell size to the photon's frequency-dependent mean free path. When the cell size is much larger than the photon's mean free path, a diffusion solution for such a frequency radiation will be obtained. On the other hand, when the cell size is much smaller than the photon's mean free path, a free transport mechanism will be recovered. In the regime between the above two limits, with the variation of the ratio between the local cell size and photon's mean free path, the UGKS provides a smooth transition in the physical and frequency space to capture the corresponding transport physics accurately. The seemingly straightforward extension of the UGKS from the gray to multiple frequency radiation system is due to its intrinsic consistent multiple scale transport modeling, but it still involves lots of work to properly discretize the multiple groups in order to design an asymptotic preserving (AP) scheme in all regimes. The current scheme is tested in a few frequency-dependent radiation problems, and the results are compared with the solutions from the well-defined implicit Monte Carlo (IMC) method. The UGKS is much more efficient than IMC, and the computational times of both schemes for all test cases are listed. The UGKS seems to be the first discrete ordinate method (DOM) for the accurate capturing of multiple frequency radiative transport physics from ballistic particle motion to the diffusive wave propagation.

* Corresponding author.
E-mail addresses: sun_wenjun@iapcm.ac.cn (W.J. Sun), jiang@iapcm.ac.cn (S. Jiang), makxu@ust.hk (K. Xu), li_shu@iapcm.ac.cn (S. Li).

http://dx.doi.org/10.1016/j.jcp.2015.09.002
0021-9991/

1. Introduction

To solve the radiative transfer equations is very challenging, but it is important in astrophysics, inertial confinement fusion, and high temperature flow systems. Due to the complexity of the system, its study attracts continuous attention from national laboratories and academic institutes. This paper presents a continuous effort to develop a useful and reliable computational method for multiple scale radiative transport system.

In a previous work, we have developed an asymptotic preserving unified gas kinetic scheme (UGKS) for the gray radiative transfer equations [22]. Here an extension of the scheme to frequency-dependent radiative transfer system will be developed. The radiative transfer equations are the modeling equations in the kinetic level, where the photon transport and collision with material are taken into account. This system can present different limiting solutions with the changing of the scales. For the gray radiative transfer equations, the opacity is just a function of the material temperature. Therefore, the spatial cells can be classified as optical thick and optical thin regions, and a domain decomposition method with different numerical discretization in different regions can be developed. However, for the frequency-dependent radiative transfer equations, the opacity is typically a decreasing function of frequency. A spatial region can be optically thick for low frequency photon, but optically thin for high frequency ones. It becomes challenging to develop a reliable asymptotic preserving scheme for simulating different frequency photon transport efficiently.

The radiative transfer equations model the radiation intensity transport and energy exchange with the background material. The properties of the background material influence greatly on the behavior of radiation transfer. For a low opacity (background) material, the interaction between the radiation and material is weak, and the radiation propagates in a transparent way. The numerical method in this regime can be well developed by tracking the particle streaming transport. However, for a high opacity (background) material, there is severe interaction between radiation and material with a diminishing photon mean free path. As a result, the diffusive radiative behavior will emerge. In order to solve the kinetic scale based radiative transfer equations numerically, a straightforward way is to use a spatial mesh size which is comparable with photon's mean-free path, i.e., the so-called optical thin cell, and the transport equation can be discretized directly, such as using upwind approach for photon transport. This kind of method is basically a single scale method, where the numerical resolution down to the mean free path is used everywhere in the computation. Most Monte Carlo methods for transport equations belong to this category as well. In this kind of methods, to take such a small cell size will be associated with huge computational cost in the optical thick regime. In order to use a large cell size in comparison with the mean free path in the optical thick region, instead of decoupling the particle transport and collision in the numerical discretization, the coupled transport and collision has to be taken into account in the design of the scheme.

One of the idealized multiscale methods is to develop the so-called asymptotic preserving (AP) scheme for the kinetic equation. When holding the mesh size and time step fixed and as the Knudsen number going to zero, the AP scheme should automatically recover the discrete diffusion solution. AP schemes were first studied in the numerical solution of steady neutron transport problems by Larsen, Morel and Miller [17], Larsen and Morel [16], and then by Jin and Levermore [10,11], and the others. For unsteady problems, one of the AP schemes was constructed based on a decomposition of the distribution function between an equilibrium part and its non-equilibrium derivation, see Klar [13,14], and Jin, Pareschi and Toscani [12] for details. The development of an AP-type discrete ordinate method (DOM) for the multi-frequency radiative transfer equation coupled with material energy equation is an extremely difficult numerical problem [7,8,21], where most well-validated approaches are the Monte Carlo methods.

The UGKS is one of the AP schemes for the transport equations [4,9,24,26]. It not only recovers accurate limiting solutions, such as ballistic transport and diffusion propagation, but also presents reliable solution in the whole transition regime. In UGKS, the mesh size is used directly as a modeling scale for identifying transport dynamics. When the mesh size is on the order of mean free path, the kinetic transport mechanism, such as the modeling process of the Boltzmann equation, is recovered in the numerical evolution [25]. When the mesh size is much larger than the mean free path, the hydrodynamic scale physics, such as the Navier–Stokes (NS) solutions for the flow system and the diffusion equation for the radiative transfer, is obtained. Between these two limits, a smooth transition is constructed and used for the capturing of non-equilibrium phenomena. In UGKS the mesh size and time step are dynamic variables in the evolution model. It may not be difficult to accept this kind of concept if we can realize that all fluid dynamic equations, such as the Boltzmann equation and the NS equations, are constructed based on their specific modeling scales with the corresponding dynamics. More or less the UGKS is using the mesh size and time step to model the dynamics and get the solutions without going through the partial differential equations step [24].

In this paper, an AP UGKS (AP-UGKS) will be developed for the frequency-dependent radiative equations, which are composed of radiation transport and material energy equation. In terms of dynamic modeling, the frequency-dependent radiation system is much more complicated. Within the same spatial cell, both optical thin and thick dynamics can appear for different frequency photons. Not only for the capturing of limiting solutions, accurate solution in the whole transition regime is required in order to capture the dynamics of a continuum spectrum in the frequency domain. The critical ingredient of UGKS is the use of an un-splitting treatment of photon's transport and collision and its automatic recovery of optical thin and thick transport mechanism. The importance of the coupling of transport and collision has been emphasized in a recent paper for the development of AP schemes [5]. The basic steps of AP-UGKS are the following. The multi-group method is first used to discretize the frequency variable, and the discrete-ordinate method (DOM) is employed to discretize the angular distribution of photon's movement. A time evolution integral solution of radiation intensity at different frequency is

constructed for the flux evaluation at a cell interface. In order to evaluate the source terms inside each cell for the radiation intensity update, the macroscopic radiation energy equations at each frequency and the material energy equation are solved first at the next time level for the update of macroscopic radiation energy and material temperature. Then, the updated macroscopic quantities are used in UGKS for the full determination of the multi-group radiation intensity inside the cell. For the multiple frequency radiative transfer, much numerical work is involved in the numerical discretization in the radiation frequency space and their coupling. Also, due to the complicated nature of such a system, we can only find the numerical examples, which have been previously tested by the Monte Carlo methods. We could not find any other DOM for the multiple frequency radiative transfer system [8,21].

This paper is organized as follows. Section 2 introduces the model equations of the frequency-dependent radiative transfer. Section 3 is the construction of the unified scheme for such a system. Section 4 gives the asymptotic preserving analysis. In Section 5 many frequency-dependent numerical tests are included to demonstrate the accuracy and robustness of the new scheme, and its efficiency comparison with Monte Carlo method. A conclusion is given in the last section.

2. System of frequency-dependent radiative transfer equations

The frequency-dependent radiative transfer equations describe the radiative transfer and the energy exchange between radiation and material. The equations can be written in following scaled form:

$$\begin{cases} \dfrac{\epsilon^2}{c}\dfrac{\partial I}{\partial t} + \epsilon\vec{\Omega}\cdot\nabla I = \sigma\big(B(\nu,T) - I\big), \\ \epsilon^2 C_\nu \dfrac{\partial T}{\partial t} \equiv \epsilon^2 \dfrac{\partial U}{\partial t} = \displaystyle\int_{4\pi}\int_0^\infty \sigma\big(I - B(\nu,T)\big)d\nu d\vec{\Omega}. \end{cases} \tag{2.1}$$

Here $I(t,\vec{r},\vec{\Omega},\nu)$ is the radiation intensity, $\vec{r}$ is the spatial variable, $\vec{\Omega}$ is the angular variable, t is the time, and $\nu\in(0,+\infty)$ is the frequency variable. Here $T(\vec{r},t)$ is the material temperature, $\sigma(\vec{r},\nu,T)$ is the opacity, c is the speed of light, $\epsilon>0$ is the Knudsen number, and $U(\vec{r},t)$ is the material energy density. For the simplicity of presentation, we have omitted the internal source and scattering terms in (2.1). In addition, the Planck function $B(\nu,T)$ is defined by

$$B(\nu,T) = \frac{2h\nu^3}{c^2}\frac{1}{e^{h\nu/kT}-1}, \tag{2.2}$$

where h is Planck's constant and k is Boltzmann's constant.

The material temperature $T(\vec{r},t)$ and the material energy density $U(\vec{r},t)$ are related by

$$\frac{\partial U}{\partial T} = C_V > 0,$$

where $C_V(\vec{r},t)$ is the heat capacity.

As the parameter $\epsilon\to 0$, Larsen et al. [18] have shown that, away from boundaries and initial times, the intensity I approaches to a Planckian at the local temperature, i.e.,

$$I^{(0)} = B(\nu,T^{(0)}),$$

and the corresponding local temperature $T^{(0)}$ satisfies the following nonlinear diffusion equation,

$$\frac{\partial}{\partial t}U(T^{(0)}) + a\frac{\partial}{\partial t}(T^{(0)})^4 = \nabla\cdot\frac{ac}{3\sigma_R}\nabla(T^{(0)})^4, \tag{2.3}$$

where a is the radiation constant given by

$$a = \frac{8\pi k^4}{15h^3c^3},$$

and σ_R is the Rosseland mean opacity defined by

$$\frac{1}{\sigma_R} = \frac{\int_0^\infty \frac{1}{\sigma(\vec{r},\nu,T)}\frac{\partial B(\nu,T)}{\partial T}d\nu}{\int_0^\infty \frac{\partial B(\nu,T)}{\partial T}d\nu}.$$

The asymptotic analysis was also presented in [2].

An asymptotic preserving (AP) scheme for the frequency-dependent radiation transfer equations (2.1) is a numerical scheme which discretizes (2.1) in such a way that it leads to a correct discretization of the diffusion limit (2.3) when ϵ is small, and the scheme should be uniformly stable in ϵ.

The limiting equation (2.3) is what we would like to get in the AP scheme for (2.1) in the optical thick region. For simplicity, we consider here the two-dimensional Cartesian spatial case for problem (2.1). Thus in this case, the angle

direction is denoted by $\vec{\Omega} = (\mu, \xi)$, with $\mu = \sqrt{1-\zeta^2}\cos\theta$, $\xi = \sqrt{1-\zeta^2}\sin\theta$, $\zeta \in [-1, 1]$ as the cosine value of the angle between the propagation direction $\vec{\Omega}$ and the z-axis, and $\theta \in [0, 2\pi)$ as the angle between the projection vector of $\vec{\Omega}$ onto the xy-plane and the x-axis. Due to the symmetry of angular distribution in the two-dimensional Cartesian case, we need to consider $\zeta \geq 0$ only.

3. UGKS for frequency-dependent radiative transfer equations

In this section, based on the UGKS framework in [9,20,22,26], we will present the AP-UGKS for the frequency-dependent radiative transfer system (2.1).

3.1. Frequency space discretization

For the system (2.1), we first give the discretization of frequency variable ν. A standard way is to apply a multi-group method. In the multi-group method, the frequency variable ν is divided into discrete frequency intervals and "groups" the photons according to these intervals [1]. Let G be the positive integer number, we discretize the continuous frequency space $(0, +\infty)$ by G discrete frequency intervals $(\nu_{g-\frac{1}{2}}, \nu_{g+\frac{1}{2}})$ with $g = 1, \cdots, G$, and $\nu_{\frac{1}{2}} = 0$, $\nu_{G+\frac{1}{2}} = +\infty$. Once the boundaries of the groups are defined, we can integrate the first equation in (2.1) over the frequency interval,

$$\int_{\nu_{g-\frac{1}{2}}}^{\nu_{g+\frac{1}{2}}} \left(\frac{\epsilon}{c}\partial_t I + \vec{\Omega}\cdot\nabla I\right) d\nu = \int_{\nu_{g-\frac{1}{2}}}^{\nu_{g+\frac{1}{2}}} \frac{\sigma}{\epsilon}\big(B(\nu, T) - I\big) d\nu. \tag{3.1}$$

For equation (3.1), the radiation intensity in different groups and the corresponding group opacities are given by

$$I_g = \int_{\nu_{g-\frac{1}{2}}}^{\nu_{g+\frac{1}{2}}} I(t, \vec{r}, \vec{\Omega}, \nu) d\nu, \tag{3.2}$$

and

$$\begin{aligned} \sigma_g^e &= \frac{\displaystyle\int_{\nu_{g-\frac{1}{2}}}^{\nu_{g+\frac{1}{2}}} \sigma B(\nu, T) d\nu}{\displaystyle\int_{\nu_{g-\frac{1}{2}}}^{\nu_{g+\frac{1}{2}}} B(\nu, T) d\nu}, \\ \sigma_g^a &= \frac{\displaystyle\int_{\nu_{g-\frac{1}{2}}}^{\nu_{g+\frac{1}{2}}} \sigma I d\nu}{\displaystyle\int_{\nu_{g-\frac{1}{2}}}^{\nu_{g+\frac{1}{2}}} I d\nu}. \end{aligned} \tag{3.3}$$

For Planck function $B(\nu, T)$ on the right hand side of equation (3.1), it is also integrated over the frequency interval

$$\phi_g = \int_{\nu_{g-\frac{1}{2}}}^{\nu_{g+\frac{1}{2}}} B(\nu, T) d\nu. \tag{3.4}$$

With these notations in (3.2), (3.3), and (3.4), equation (2.1) goes to an equivalent multi-group radiative transfer system:

$$\begin{cases} \dfrac{\epsilon^2}{c}\dfrac{\partial I_g}{\partial t} + \epsilon\vec{\Omega}\cdot\nabla I_g = (\sigma_g^e\phi_g - \sigma_g^a I_g) \quad (g = 1, \cdots, G), \\ \epsilon^2 C_v \dfrac{\partial T}{\partial t} \equiv \epsilon^2 \dfrac{\partial U}{\partial t} = \displaystyle\sum_{g=1}^{g=G} \int_{4\pi} (\sigma_g^a I_g - \sigma_g^e \phi_g) d\vec{\Omega}. \end{cases} \tag{3.5}$$

It should be pointed out that the absorption opacity σ_g^a is a weighted integration with the unknown function I. Usually, the unknown function I in this opacity integration is replaced by the Planck function with the radiation temperature T_r instead of the material temperature T. For this purpose, we define the radiation temperature and the absorption opacity in the following ways,

$$
\begin{aligned}
&acT_r^4 = \int_{4\pi}\int_0^{+\infty} Id\vec{\Omega}d\nu = \sum_{g=1}^{g=G}\int_{4\pi} I_g d\vec{\Omega},\\
&\sigma_g^a = \frac{\int_{\nu_{g-\frac{1}{2}}}^{\nu_{g+\frac{1}{2}}} \sigma B(\nu, T_r)d\nu}{\int_{\nu_{g-\frac{1}{2}}}^{\nu_{g+\frac{1}{2}}} B(\nu, T_r)d\nu}.
\end{aligned}
\tag{3.6}
$$

Up to now, the discretization of the frequency variable is finished.

3.2. Discrete ordinate method

For the angular variable, as done for the usual discrete ordinate method for equation (3.5), we first give the propagation direction (μ, ξ) a discrete value. As in [19] for example, we use the even integer N as the discrete ordinate order, then obtain the discrete directions $\vec{\Omega}_m \triangleq (\mu_m, \xi_m)$ and their corresponding integration weights ω_m for $m = 1, \cdots, M$, with $M = N(N+2)/2$. For each direction (μ_m, ξ_m), we get the discrete equation for the multi-group radiative transfer equations (3.5):

$$
\begin{cases}
\dfrac{\epsilon^2}{c}\dfrac{\partial I_{m,g}}{\partial t} + \epsilon\vec{\Omega}_m\cdot\nabla I_{m,g} = (\sigma_g^e\phi_g - \sigma_g^a I_{m,g}) \quad (g = 1, \cdots, G,\ m = 1, \cdots, M),\\
\epsilon^2 C_v\dfrac{\partial T}{\partial t} \equiv \epsilon^2\dfrac{\partial U}{\partial t} = \displaystyle\sum_{g=1}^{g=G}\sum_{m=1}^{m=M}(\sigma_g^a I_{m,g} - \sigma_g^e\phi_g)\omega_m.
\end{cases}
\tag{3.7}
$$

Let $x_i = i\Delta x$, $y_j = j\Delta y$ and $t^n = n\Delta t$ $(i, j, n \in \mathbb{Z})$ be the uniform mesh in Cartesian coordinates, where $\Delta x, \Delta y$ and Δt are the mesh sizes in the x-, y-directions and the time step in t-direction. Let (i, j) denote the cell $\{(x, y);\ x_{i-1/2} < x < x_{i+1/2},\ y_{j-1/2} < y < y_{j+1/2}\}$, where $x_{i-1/2} = (i - \frac{1}{2})\Delta x$ and $y_{j-1/2} = (j - \frac{1}{2})\Delta y$ are the cell interfaces.

In the following, we use the notation $I^n_{i,j,m,g}$ as the cell averaged value of intensity variable $I_{m,g}$ at time t^n in cell (i, j) with cell center (x_i, y_j). Then, we integrate equation (3.7) over the cell (i, j) from time t^n to $t^n + \Delta t$. A conservative finite volume numerical scheme for the equation (3.7) is of the form

$$
\begin{cases}
I^{n+1}_{i,j,m,g} = I^n_{i,j,m,g} + \dfrac{\Delta t}{\Delta x}(F_{i-1/2,j,m,g} - F_{i+1/2,j,m,g}) + \dfrac{\Delta t}{\Delta y}(H_{i,j-1/2,m,g} - H_{i,j+1/2,m,g})\\
\qquad\qquad + \dfrac{c\Delta t}{\epsilon^2}\left\{(\sigma_g^e\tilde{\phi}_{g,i,j} - \sigma_g^a\tilde{I}_{i,j,m,g})\right\},\\
\epsilon^2 C_v T^{n+1}_{i,j} = \epsilon^2 C_v T^n_{i,j} + \Delta t\displaystyle\sum_{g=1}^{g=G}\sum_{m=1}^{m=M}(\sigma_g^a\tilde{I}_{i,j,m,g} - \sigma_g^e\tilde{\phi}_{g,i,j})\omega_m,
\end{cases}
\tag{3.8}
$$

where $F_{i-1/2,j,m,g}$ and $H_{i,j-1/2,m,g}$ are the time-dependent numerical fluxes in the x- and y-directions across the cell interfaces. And the terms in the equations of (3.8) are given by

$$
\begin{aligned}
&F_{i-1/2,j,m,g} = \frac{c}{\epsilon\Delta t}\int_{t^n}^{t^{n+1}} \mu_m I_{m,g}(t, x_{i-\frac{1}{2}}, y_j, \mu_m, \xi_m)dt,\\
&H_{i,j-1/2,m,g} = \frac{c}{\epsilon\Delta t}\int_{t^n}^{t^{n+1}} \xi_m I_{m,g}(t, x_i, y_{j-\frac{1}{2}}, \mu_m, \xi_m)dt,\\
&\tilde{\phi}_{g,i,j} = \frac{1}{\Delta t\Delta x\Delta y}\int_{t^n}^{t^{n+1}}\int_{x_{i-1/2}}^{x_{i+1/2}}\int_{y_{j-1/2}}^{y_{j+1/2}} \phi_g(t, x, y)dxdydt,
\end{aligned}
$$

$$\tilde{I}_{i,j,m,g} = \frac{1}{\Delta x \Delta y \Delta t} \int_{t^n}^{t^{n+1}} \int_{x_{i-1/2}}^{x_{i+1/2}} \int_{y_{j-1/2}}^{y_{j+1/2}} I_{m,g}(t, x, y, \mu_m, \xi_m) dx dy dt. \tag{3.9}$$

In order to update the system (3.8), we need to determine all terms in (3.9) explicitly. First, the term $\tilde{I}_{i,j,m,g}$ in (3.9) can be approximated implicitly by

$$\tilde{I}_{i,j,m,g} \approx I^{n+1}_{i,j,m,g},$$

which can be combined with the solution on the left hand side of Eq. (3.8).

3.3. UGKS: microscopic inner loop

The key for UGKS is to model the time-dependent interface fluxes $F_{i-1/2,j,m,g}$ and $H_{i,j-1/2,m,g}$ in Eq. (3.9). The radiation intensity at a cell interface is based on an evolution solution of the transport equation with initial value $I^n_{i,j,m,g}$ [20,22,26]. This evolution solution covers different flow regimes from the ballistic transport to the hydrodynamic wave propagation [24]. The real solution used for the flux evaluation depends on the ratio of the time step to the local particle collision time.

For the x-direction flux $F_{i-1/2,j,m,g}$, the radiation intensity is obtained by solving the following initial value problem at the cell boundary $x = x_{i-1/2}$, $y = y_j$:

$$\begin{cases} \dfrac{\epsilon}{c}\partial_t I_{m,g} + \mu_m \partial_x I_{m,g} = \dfrac{1}{\epsilon}(\sigma^e_g \phi_g - \sigma^a_g I_{m,g}), \\ I_{m,g}(x, y_j, t)|_{t=t^n} = I_{m,g,0}(x, y_j, t^n). \end{cases} \tag{3.10}$$

Thus, a time-dependent evolution solution can be obtained,

$$\begin{aligned} I_{m,g}(t, x_{i-1/2}, y_j, \mu_m, \xi_m) = {} & e^{-\lambda_{g,i-1/2,j}(t-t^n)} I_{m,g,0}\left(x_{i-1/2} - \frac{c\mu_m}{\epsilon}(t-t^n)\right) \\ & + \int_{t^n}^{t} e^{-\lambda_{g,i-1/2,j}(t-s)} \frac{c\sigma^e_{g,i-1/2,j}}{\epsilon^2} \phi_g\left(s, x_{i-1/2} - \frac{c\mu_m}{\epsilon}(t-s)\right) ds, \end{aligned} \tag{3.11}$$

where $\lambda_g = c\sigma^a_g/\epsilon^2$ and $\lambda_{g,i-1/2,j}$ denote the value of λ_g at the corresponding cell boundary. Substituting $I_{m,g}(t, x_{i-1/2}, y_j, \mu_m, \xi_m)$ of (3.11) into (3.9), and integrating it with respect to time t from t^n to t^{n+1}, we can get the numerical flux $F_{i-1/2,j,m,g}$ in the x-direction. The numerical flux $H_{i,j-1/2,m,g}$ in the y-direction can be constructed similarly.

The solution in Eq. (3.11) depends on two functions, which need to be modeled numerically. The first one is $I_{m,g}(t, x, y_j)$ at t^n around $(x_{i-1/2}, y_j)$, which is the initial condition for function $I_{m,g,0}(x, y_j, t^n)$, and the other one is the function $\phi_g(t, x, y)$ between the time steps t^n and t^{n+1} around the cell boundary $(x_{i-1/2}, y_j)$.

The initial condition $I_{m,g,0}(x, y_j, t^n)$ at the beginning of each time step in (3.10) can be approximated by a piecewise linear function:

$$I_{m,g,0}(x, y_j, t^n) = \begin{cases} I^n_{i-1,j,m,g} + \delta_x I^n_{i-1,j,m,g}(x - x_{i-1}), & \text{if } x < x_{i-1/2}, \\ I^n_{i,j,m,g} + \delta_x I^n_{i,j,m,g}(x - x_i), & \text{if } x > x_{i-1/2}. \end{cases} \tag{3.12}$$

Here $\delta_x I^n_{i-1,j,m,g}$, $\delta_x I^n_{i+1,j,m,g}$ are the reconstructed slopes through the second order MUSCL limiter [23].

The function $\phi_g(x, y_j, t)$ between the time steps t^n and t^{n+1} around the cell boundary $(x_{i-1/2}, y_j)$ is modeled by a piecewise continuous polynomial as:

$$\begin{aligned} \phi_g(x, y_j, t) = {} & \phi^{n+1}_{g,i-1/2,j} + \delta_t \phi^{n+1}_{g,i-1/2,j}(t - t^{n+1}) \\ & + \begin{cases} \delta_x \phi^{n+1,L}_{g,i-1/2,j}(x - x_{i-1/2}), & \text{if } x < x_{i-1/2}, \\ \delta_x \phi^{n+1,R}_{g,i-1/2,j}(x - x_{i-1/2}), & \text{if } x > x_{i-1/2}. \end{cases} \end{aligned} \tag{3.13}$$

Here the left and right one-sided finite differences are given by

$$\delta_x \phi^{n+1,L}_{g,i-1/2,j} = \frac{\phi^{n+1}_{g,i-1/2,j} - \phi^{n+1}_{g,i-1,j}}{\Delta x/2}, \qquad \delta_x \phi^{n+1,R}_{g,i-1/2,j} = \frac{\phi^{n+1}_{g,i,j} - \phi^{n+1}_{g,i-1/2,j}}{\Delta x/2}.$$

And for the time derivative $\delta_t \phi^{n+1}_{g,i-1/2,j}$, we use

$$\delta_t \phi^{n+1}_{g,i-1/2,j} = \frac{\phi^{n+1}_{g,i-1/2,j} - \phi^{n}_{g,i-1/2,j}}{\Delta t}.$$

The cell boundary value $\phi^{n+1}_{g,i-1/2,j}$ and the cell center values $\phi^{n+1}_{g,i,j}$ and $\phi^{n+1}_{g,i-1,j}$ will be determined later. Given the above constructions, the numerical flux

$$F_{i-1/2,j,m,g} = \frac{c\mu_m}{\epsilon\Delta t}\int_{t^n}^{t^{n+1}} I_{m,g}(t, x_{i-1/2}, y_j, \mu_m, \xi_m)dt$$

can be exactly computed by using the expressions (3.11), (3.12) and (3.13),

$$\begin{aligned} F_{i-1/2,j,m,g} = {} & A_{g,i-1/2,j}\mu_m(I^-_{i-1/2,j,m,g}1_{\mu_m>0} + I^+_{i-1/2,j,m,g}1_{\mu_m<0}) + C_{g,i-1/2,j}\mu_m\phi^{n+1}_{g,i-1/2,j} \\ & + D_{g,i-1/2,j}(\mu_m^2\delta_x\phi^{n+1,L}_{g,i-1/2,j}1_{\mu_m>0} + \mu_m^2\delta_x\phi^{n+1,R}_{g,i-1/2,j}1_{\mu_m<0}) \\ & + B_{g,i-1/2,j}(\mu_m^2\delta_x I^n_{i-1,j,m,g}1_{\mu_m>0} + \mu_m^2\delta_x I^n_{i,j,m,g}1_{\mu_m<0}) \\ & + E_{g,i-1/2,j}\mu_m\delta_t\phi^{n+1}_{g,i-1/2,j}, \end{aligned} \tag{3.14}$$

where $I^-_{i-1/2,j,m,g}$ and $I^+_{i-1/2,j,m,g}$ are values at boundary, which are given by

$$\begin{aligned} I^-_{i-1/2,j,m,g} &= I_{i-1,j,m,g} + \frac{\Delta x}{2}\delta_x I^n_{i-1,j,m,g}, \\ I^+_{i-1/2,j,m,g} &= I_{i,j,m,g} - \frac{\Delta x}{2}\delta_x I^n_{i,j,m,g}. \end{aligned}$$

The coefficients in (3.14) are

$$\begin{aligned} A_g &= \frac{c}{\epsilon\Delta t\lambda_g}(1-e^{-\lambda_g\Delta t}), \\ C_g &= \frac{c^2\sigma^e_g}{\Delta t\epsilon^3\lambda_g}\left(\Delta t - \frac{1}{\lambda_g}(1-e^{-\lambda_g\Delta t})\right), \\ D_g &= -\frac{c^3\sigma^e_g}{\Delta t\epsilon^4\lambda_g^2}\left(\Delta t(1+e^{-\lambda_g\Delta t}) - \frac{2}{\lambda_g}(1-e^{-\lambda_g\Delta t})\right), \\ B_g &= -\frac{c^2}{\epsilon^2\lambda_g^2\Delta t}(1-e^{-\lambda_g\Delta t} - \lambda_g\Delta t e^{-\lambda_g\Delta t}), \\ E_g &= \frac{c^2\sigma^e_g}{\epsilon^3\lambda_g^3\Delta t}\left(1-e^{-\lambda_g\Delta t} - \lambda_g\Delta t e^{-\lambda_g\Delta t} - \frac{1}{2}(\lambda\Delta t)^2\right), \end{aligned} \tag{3.15}$$

with $\lambda_g = c\sigma^a_g/\epsilon^2$. With the expression (3.15), we have

$$\begin{aligned} A_{g,i-1/2,j} &= A_g(\Delta t, \epsilon, \lambda_{g,i-1/2,j}), \\ C_{g,i-1/2,j} &= C_g(\Delta t, \epsilon, \sigma^e_{g,i-1/2,j}, \lambda_{g,i-1/2,j}), \\ D_{g,i-1/2,j} &= D_g(\Delta t, \epsilon, \sigma^e_{g,i-1/2,j}, \lambda_{g,i-1/2,j}), \\ B_{g,i-1/2,j} &= B_g(\Delta t, \epsilon, \lambda_{g,i-1/2,j}), \\ E_{g,i-1/2,j} &= E_g(\Delta t, \epsilon, \sigma^e_{g,i-1/2,j}, \lambda_{g,i-1/2,j}). \end{aligned} \tag{3.16}$$

It should be emphasized here that even with the interface solution (3.11), in order to obtain a consistent limiting diffusive flux, the coefficients, such as $\sigma^e_{g,i-1/2,j}$ and $\lambda_{g,i-1/2,j}$ at a cell boundary, have to be properly defined by using the values from the two neighboring cells in the above expression (3.16).

The boundary flux $H_{i,j-\frac{1}{2},m,g}$ in the y-direction can be constructed in the same way. This completes the construction of the numerical boundary fluxes for multi-group radiative transfer equations (3.8).

3.4. UGKS: macroscopic inner loop

To complete the construction of numerical scheme for (3.7), the detailed expressions $\tilde{\phi}_g$ in (3.8), and $\phi^{n+1}_{g,i-1/2,j}$, $\phi^{n+1}_{g,i,j}$, and $\phi^{n+1}_{g,i-1,j}$ in (3.13), have to be given. Following the methodology of UGKS, we will first evaluate the macroscopic radiation energy and material temperature at next time level through the following macroscopic equations. First, let's take the angular integration of the first equation in (3.5) and obtain the following system for macroscopic variables:

$$\begin{cases} \dfrac{\epsilon^2}{c}\dfrac{\partial \rho_g}{\partial t} + \epsilon \nabla \cdot \langle \vec{\Omega} I_g \rangle = (4\pi \sigma_g^e \phi_g - \sigma_g^a \rho_g) \quad (g = 1, \cdots, G), \\ \epsilon^2 C_v \dfrac{\partial T}{\partial t} \equiv \epsilon^2 \dfrac{\partial U}{\partial t} = \displaystyle\sum_{g=1}^{g=G} (\sigma_g^a \rho_g - 4\pi \sigma_g^e \phi_g), \end{cases} \tag{3.17}$$

where $\rho_g = \int_{4\pi} I_g d\vec{\Omega}$ and $\langle \vec{\Omega} I_g \rangle$ is the angular vector integration given by

$$\langle \vec{\Omega} I_g \rangle = \int_{4\pi} \vec{\Omega} I_g d\vec{\Omega}.$$

The numerical discretization for the above macroscopic equations (3.17) can be written as

$$\begin{cases} \rho_{g,i,j}^{n+1} = \rho_{g,i,j}^{n} + \dfrac{\Delta t}{\Delta x}(\Phi_{g,i-1/2,j}^{n+1} - \Phi_{g,i+1/2,j}^{n+1}) + \dfrac{\Delta t}{\Delta y}(\Psi_{g,i,j-1/2}^{n+1} - \Psi_{g,i,j+1/2}^{n+1}) \\ \qquad + \dfrac{c\Delta t}{\epsilon^2}\left(4\pi (\sigma_g^e)_{i,j}^{n+1} \phi_{g,i,j}^{n+1} - (\sigma_g^a)_{i,j}^{n+1} \rho_{g,i,j}^{n+1}\right) \quad (g = 1, \cdots, G) \\ C_v T_{i,j}^{n+1} = C_v T_{i,j}^{n} + \dfrac{\Delta t}{\epsilon^2} \displaystyle\sum_{g=1}^{g=G} \left((\sigma_g^a)_{i,j}^{n+1} \rho_{g,i,j}^{n+1} - 4\pi (\sigma_g^e)_{i,j}^{n+1} \phi_{g,i,j}^{n+1}\right), \end{cases} \tag{3.18}$$

where the cell interface fluxes are given by

$$\begin{aligned} \Phi_{g,i-1/2,j}^{n+1} &= \frac{c}{\epsilon \Delta t} \int_{t^n}^{t^n+\Delta t} \langle \Omega_x I_g \rangle (x_{i-1/2}, y_j, t) dt, \\ \Phi_{g,i+1/2,j}^{n+1} &= \frac{c}{\epsilon \Delta t} \int_{t^n}^{t^n+\Delta t} \langle \Omega_x I_g \rangle (x_{i+1/2}, y_j, t) dt, \\ \Psi_{g,i,j-1/2}^{n+1} &= \frac{c}{\epsilon \Delta t} \int_{t^n}^{t^n+\Delta t} \langle \Omega_y I_g \rangle (x_i, y_{j-1/2}, t) dt, \\ \Psi_{g,i,j+1/2}^{n+1} &= \frac{c}{\epsilon \Delta t} \int_{t^n}^{t^n+\Delta t} \langle \Omega_y I_g \rangle (x_i, y_{j+1/2}, t) dt. \end{aligned} \tag{3.19}$$

With the cell interface intensity I_g $(g = 1, \cdots, G)$ in (3.11), we can get the explicit expression for all terms in (3.19). For example, at the cell interface in the x-direction, we can get

$$\begin{aligned} \Phi_{g,i-1/2,j}^{n+1} &= \frac{c}{\epsilon \Delta t} \int_{t^n}^{t^n+\Delta t} \langle \Omega_x I_g \rangle (x_{i-1/2}, y_j, t) dt \\ &= \sum_{m=1}^{M} \omega_m F_{i-1/2,j,m,g} \\ &= A_{g,i-1/2,j}^{n+1} \sum_{m=1}^{M} \omega_m \mu_m (I_{i-1,j,m,g}^{n} 1_{\mu_m > 0} + I_{i,j,m,g}^{n} 1_{\mu_m < 0}) \\ &\quad + \frac{4\pi D_{g,i-1/2,j}^{n+1}}{3} \left(\frac{\phi_{g,i,j}^{n+1} - \phi_{g,i-1,j}^{n+1}}{\Delta x} \right) \\ &\quad + B_{g,i-1/2,j}^{n+1} \sum_{m=1}^{M} \omega_m \mu_m^2 (\delta_x I_{i-1,j,m,g}^{n} 1_{\mu_m > 0} + \delta_x I_{i,j,m,g}^{n} 1_{\mu_m < 0}), \end{aligned} \tag{3.20}$$

where the expressions of $A_{g,i-1/2,j}^{n+1}$, $B_{g,i-1/2,j}^{n+1}$ and $D_{g,i-1/2,j}^{n+1}$ in (3.20) are the same as the parameters $A_{g,i-1/2,j}$, $B_{g,i-1/2,j}$, and $D_{g,i-1/2,j}$ in (3.16), but with the following definitions for the cell interface values $(\sigma_g^a)_{i-1/2,j}$ and $(\sigma_g^e)_{i-1/2,j}$,

$$(\sigma_g^a)_{i-1/2,j}^{n+1} = \frac{2(\sigma_g^a)_{i,j}^{n+1}(\sigma_g^a)_{i-1,j}^{n+1}}{(\sigma_g^a)_{i,j}^{n+1} + (\sigma_g^a)_{i-1,j}^{n+1}},$$
$$(\sigma_g^e)_{i-1/2,j}^{n+1} = \frac{2(\sigma_g^e)_{i,j}^{n+1}(\sigma_g^e)_{i-1,j}^{n+1}}{(\sigma_g^e)_{i,j}^{n+1} + (\sigma_g^e)_{i-1,j}^{n+1}}. \tag{3.21}$$

Up to now, with the given interface fluxes in (3.19), the equations (3.18) become a coupled nonlinear system for the macroscopic quantities $T_{i,j}^{n+1}$ and $\rho_{g,i,j}^{n+1}$ $(g = 1, \cdots, G)$, where the parameters $(\sigma_g^a)_{i,j}^{n+1}$ and $(\sigma_g^e)_{i,j}^{n+1}$ depend implicitly on the material temperature $T_{i,j}^{n+1}$. This nonlinear system can be solved by an iterative method, which is given below.

Algorithm for solving (3.18). Based on the initial radiation intensity $I_{i,j,m,g}^n$ and $T_{i,j}^n$, we have $\rho_{g,i,j}^n$ and $\phi_{g,i,j}^n$. Find $\rho_{g,i,j}^{n+1}$ and $T_{i,j}^{n+1}$ in equations (3.18).

1) Set the initial iterative value $\rho_{g,i,j}^{n+1,0} = \rho_{g,i,j}^n$ and $T_{i,j}^{n+1,0} = T_{i,j}^n$;
2) For $s = 0, \cdots, S$.
   2.1) Compute the coefficients $(\sigma_g^a)_{i,j}^{n+1,s}$, $(\sigma_g^e)_{i,j}^{n+1,s}$, $A_{g,i-1/2,j}^{n+1,s}$, $B_{g,i-1/2,j}^{n+1,s}$ and $D_{g,i-1/2,j}^{n+1,s}$, which are functions of $T_{i,j}^{n+1,s}$.
   2.2) Find $\rho_{g,i,j}^{n+1,s+1}$ and $T_{i,j}^{n+1,s+1}$ of the following iterative system:

$$\begin{cases} \rho_{g,i,j}^{n+1,s+1} = \rho_{g,i,j}^n + \dfrac{\Delta t}{\Delta x}(\Phi_{g,i-1/2,j}^{n+1,s} - \Phi_{g,i+1/2,j}^{n+1,s}) + \dfrac{\Delta t}{\Delta y}(\Psi_{g,i,j-1/2}^{n+1,s} - \Psi_{g,i,j+1/2}^{n+1,s}) \\ \qquad + \dfrac{c\Delta t}{\epsilon^2}\big(4\pi(\sigma_g^e)_{i,j}^{n+1,s}\bar{\phi}_{g,i,j}^{n+1,s+1} - (\sigma_g^a)_{i,j}^{n+1,s}\rho_{g,i,j}^{n+1,s+1}\big), \\ C_v T_{i,j}^{n+1,s+1} = C_v T_{i,j}^n + \dfrac{\Delta t}{\epsilon^2}\displaystyle\sum_{g=1}^{G=G}\big((\sigma_g^a)_{i,j}^{n+1,s}\rho_{g,i,j}^{n+1,s+1} - 4\pi(\sigma_g^e)_{i,j}^{n+1,s}\bar{\phi}_{g,i,j}^{n+1,s+1}\big), \\ \bar{\phi}_{g,i,j}^{n+1,s+1} = \phi_{g,i,j}^{n+1,s} + \left(\dfrac{\partial\phi_g}{\partial T}\right)_{i,j}^{n+1,s}(T_{i,j}^{n+1,s+1} - T_{i,j}^{n+1,s}), \\ \dfrac{\partial\phi_g}{\partial T} = \displaystyle\int_{\nu_{g-\frac{1}{2}}}^{\nu_{g+\frac{1}{2}}} \frac{\partial B(\nu,T)}{\partial T}d\nu, \end{cases} \tag{3.22}$$

   where $(\partial\phi_g/\partial T)_{i,j}^{n+1,s}$ is a function of $T_{i,j}^{n+1,s}$, and the interface numerical flux $\Phi_{g,i-1/2,j}^{n+1,s}$ has the same form as (3.20), which can be written as

$$\begin{aligned} \Phi_{g,i-1/2,j}^{n+1,s} = {} & A_{g,i-1/2,j}^{n+1,s}\sum_{m=1}^{M}\omega_m\mu_m(I_{i-1,j,m,g}^n 1_{\mu_m>0} + I_{i,j,m,g}^n 1_{\mu_m<0}) \\ & + \frac{4\pi D_{g,i-1/2,j}^{n+1,s}}{3}\left(\frac{\phi_{g,i,j}^{n+1,s+1} - \phi_{g,i-1,j}^{n+1,s+1}}{\Delta x}\right) \\ & + B_{g,i-1/2,j}^{n+1,s}\sum_{m=1}^{M}\omega_m\mu_m^2(\delta_x I_{i-1,j,m,g}^n 1_{\mu_m>0} + \delta_x I_{i,j,m,g}^n 1_{\mu_m<0}). \end{aligned}$$

   2.3) For the system (3.22), use the Gauss–Sedel iteration to solve the resulting linear algebraic equations.
   2.4) Compute the relative iteration error. Stop the iteration when convergent condition is reached.
3) Update the solutions $\rho_{g,i,j}^{n+1} = \rho_{g,i,j}^{n+1,s+1}$ $(g = 1, \cdots, G)$ and $T_{i,j}^{n+1} = T_{i,j}^{n+1,s+1}$.

End

After obtaining $T_{i,j}^{n+1}$ in the macroscopic variable equations (3.17), we get $\phi_{g,i,j}^{n+1}$ $(g = 1, \cdots, G)$ through (3.4). Then, $\tilde{\phi}_{g,i,j}$ in (3.9) is set by

$$\tilde{\phi}_{g,i,j} = \phi_{g,i,j}^{n+1}, \tag{3.23}$$

and the cell interface value $\phi_{g,i-1/2,j}^{n+1}$ in (3.13) takes

$$\phi_{g,i-1/2,j}^{n+1} = \frac{1}{2}(\phi_{g,i-1,j}^{n+1} + \phi_{g,i,j}^{n+1}) \quad (g = 1, \cdots, G). \tag{3.24}$$

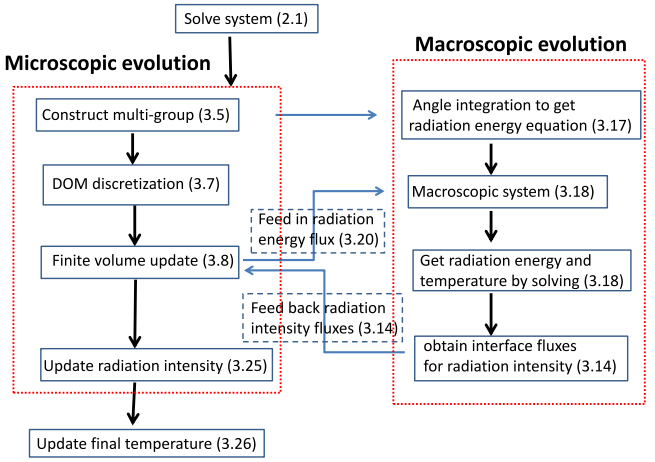

Fig. 1. The flowchart of UGKS.

The cell interface opacities $(\sigma_g^a)_{i-1/2,j}$ and $(\sigma_g^e)_{i-1/2,j}$ are determined by (3.21) with the above updated material temperature $T_{i,j}^{n+1}$ from the macro equations (3.17).

3.5. UGKS: update of radiation intensity

With the determination of the macroscopic radiation energy $\rho_{g,i,j}^{n+1}$ and material temperature $T_{i,j}^{n+1}$ at the next time level, the interface flux function for the radiation intensity of the system (3.9) is fully obtained. The radiative transfer equation in (3.7) can be solved by the following scheme

$$I_{i,j,m,g}^{n+1} = I_{i,j,m,g}^{n} + \frac{\Delta t}{\Delta x}(F_{i-1/2,j,m,g} - F_{i+1/2,j,m,g}) + \frac{\Delta t}{\Delta y}(H_{i,j-1/2,m,g} - H_{i,j+1/2,m,g}) + \frac{c\Delta t}{\epsilon^2}\left((\sigma_g^e)_{i,j}^{n+1}\phi_{g,i,j}^{n+1} - (\sigma_g^a)_{i,j}^{n+1} I_{i,j,m,g}^{n+1}\right), \tag{3.25}$$

where the opacities $(\sigma_g^e)_{i,j}^{n+1}$ and $(\sigma_g^a)_{i,j}^{n+1}$ are fully defined by the updated material temperature $T_{i,j}^{n+1}$ of the macro equations (3.17).

The final step is to solve the second equation of (3.7) to obtain the final material temperature with the newly updated value $I_{i,j,m,g}^{n+1}$. This material temperature is directly given by

$$T_{i,j}^{n+1} = \frac{C_v T_{i,j}^{n} + \Delta t \sum_{g=1}^{g=G}\sum_{m=1}^{M} \omega_m ((\sigma_g^a)_{i,j}^{n+1} I_{i,j,m,g}^{n+1} - (\sigma_g^e)_{i,j}^{n+1}\phi_{g,i,j}^{n+1})/\epsilon^2}{C_v}. \tag{3.26}$$

This completes the construction of the AP-UGKS for the frequency-dependent radiation transfer equations (2.1). We summarize the steps of AP-UGKS.

Loop of the AP-UGKS. Given $I_{i,j,m,g}^{n}$ and $T_{i,j}^{n}$ at time step n, evaluate $\rho_{g,i,j}^{n}$ and $\phi_{g,i,j}^{n}$, and find $I_{i,j,m,g}^{n+1}$ and $T_{i,j}^{n+1}$ at time step $n+1$.

1) Solve the system (3.18) to obtain $T_{i,j}^{n+1}$ and $\rho_{g,i,j}^{n+1}$, then $\phi_{g,i,j}^{n+1}$;
2) Use the obtained values $T_{i,j}^{n+1}$ and $\phi_{g,i,j}^{n+1}$ from the above step, to solve the resulting equation (3.25) to get $I_{i,j,m,g}^{n+1}$;
3) Based on the solution $I_{i,j,m,g}^{n+1}$, to get the new value $T_{i,j}^{n+1}$ by using the explicit expression (3.26);
4) Goto 1) for the next computational step.

In order to understand the algorithm clearly, the flowchart for the computation procedures is given in Fig. 1.

4. Asymptotic analysis of UGKS

In this section, we shall analyze the asymptotic properties of the UGKS for radiative transfer system. The methods in [20,22] will be used for the analysis. The property of the scheme is mainly determined by the numerical flux, which is controlled through the ϵ-dependent coefficients in (3.16). These coefficient functions satisfy the following Proposition 1.

Proposition 1. *Let the multi-group opacities σ_g^e and σ_g^a be positive. Then as ϵ tends to zero, we have*

- $A_g(\Delta t, \epsilon, \lambda_g)$ *tends to 0;*
- $B_g(\Delta t, \epsilon, \lambda_g)$ *tends to 0;*
- $D_g(\Delta t, \epsilon, \sigma_g^e, \lambda_g)$ *tends to* $-c\sigma_g^e/((\sigma_g^a)^2)$.

Thus, the corresponding macroscopic diffusion flux $(\text{Diff})_{g,i-1/2,j}^{n+1}$, defined by

$$\begin{aligned}(\text{Diff})_{g,i-1/2,j}^{n+1} &= \left\langle \frac{c\mu}{\epsilon\Delta t}\int_{t^n}^{t^{n+1}} I_g(t, x_{i-1/2}, y_j, \mu, \xi)dt \right\rangle \\ &= \int_{4\pi} \frac{c\mu}{\epsilon\Delta t}\int_{t^n}^{t^{n+1}} I_g(t, x_{i-1/2}, y_j, \mu, \xi)dtd\mu d\xi,\end{aligned} \tag{4.1}$$

has the limiting solution

$$\begin{aligned}(\text{Diff})_{g,i-1/2,j}^{n+1} &= \sum_{m=1}^{M} \omega_m\mu_m I_{m,g}(t, x_{i-1/2}, y_j, \mu_m, \xi_m) \\ &\xrightarrow[\epsilon\to 0]{} -4\pi\left(\frac{c\sigma_{g,i-1/2,j}^e}{6(\sigma_{g,i-1/2,j}^a)^2}\delta_x\phi_{g,i-1/2,j}^{n+1,L} + \frac{c\sigma_{g,i-1/2,j}^e}{6(\sigma_{g,i-1/2,j}^a)^2}\delta_x\phi_{g,i-1/2,j}^{n+1,R}\right) \\ &= -\frac{4\pi c\sigma_{g,i-1/2,j}^e}{3(\sigma_{g,i-1/2,j}^a)^2}\frac{\phi_{i,j}^{n+1} - \phi_{i-1,j}^{n+1}}{\Delta x}.\end{aligned} \tag{4.2}$$

The limiting solution (4.2) gives the numerical flux of an asymptotic diffusion equation, the so-called standard three points scheme for the diffusive flux in the one-dimensional case. It will become the five points scheme in the two-dimensional case.

With the Proposition 1 and the relation (4.2), it can be shown that the UGKS constructed in the last section is an asymptotic preserving method through the following Proposition 2.

Proposition 2. *Let parameter σ be positive. Then, as ϵ tends to zero, the numerical scheme given by (3.18), (3.25), and (3.26) approaches to the standard implicit diffusion scheme for the diffusion limit equation (2.3).*

Proof. Firstly, on the order of ϵ^{-2} in (3.25), as the parameter ϵ tends to zero, we have

$$(\sigma_g^a)_{i,j}^{n+1} I_{i,j,m,g}^{n+1} \to (\sigma_g^e)_{i,j}^{n+1}\phi_{g,i,j}^{n+1}.$$

Summing the above equation over the group index g, and by the definitions of σ_g^a and σ_g^e in (3.3), we get

$$\int_0^{+\infty} \sigma I(t^{n+1}, \vec{r}_{i,j}, \vec{\Omega}_m, \nu)d\nu \to \int_0^{+\infty} \sigma B(t^{n+1}, \nu, T_{i,j}^{n+1})d\nu,$$

which implies

$$\begin{aligned}&I_{i,j,m,g}^{n+1} \to \phi_{g,i,j}^{n+1} \quad (g = 1, \cdots, G,\ m = 1, \cdots, M), \\ &(\sigma_g^a)_{i,j}^{n+1} \to (\sigma_g^p)_{i,j}^{n+1}, \\ &(\sigma_g^e)_{i,j}^{n+1} \to (\sigma_g^p)_{i,j}^{n+1} = \frac{\int_{\nu_{g-\frac{1}{2}}}^{\nu_{g+\frac{1}{2}}} \sigma(\nu, T_{i,j}^{n+1})B(\nu, T_{i,j}^{n+1})d\nu}{\int_{\nu_{g-\frac{1}{2}}}^{\nu_{g+\frac{1}{2}}} B(\nu, T_{i,j}^{n+1})d\nu}.\end{aligned} \tag{4.3}$$

Multiplying the first equation with integration weighting function ω_m and summing the resulting equation over the angle variable, then as $\epsilon \to 0$, we have

$$\rho_{g,i,j}^{n+1} \to 4\pi\phi_{g,i,j}^{n+1}. \tag{4.4}$$

Secondly, on the order of ϵ^{-1} in (3.25), such as the flux $F^{n+1}_{i-1/2,j,m,g}$ given by (3.14), the macro flux $\Phi^{n+1}_{g,i-1/2,j}$ in equation (3.20) can be obtained by multiplying the flux $F^{n+1}_{i-1/2,j,m,g}$ with the integration weight ω_m and summing over the angle variable. By Proposition 1, as $\epsilon \to 0$ we get

$$\Phi^{n+1}_{g,i-1/2,j} \to -\frac{4\pi c(\sigma^e_g)^{n+1}_{i-1/2,j}}{3[(\sigma^a_g)^{n+1}_{i-1/2,j}]^2}\frac{\phi^{n+1}_{g,i,j}-\phi^{n+1}_{g,i-1,j}}{\Delta x} = -\frac{4\pi c}{3(\sigma^p_g)^{n+1}_{i-1/2,j}}\frac{\phi^{n+1}_{g,i,j}-\phi^{n+1}_{g,i-1,j}}{\Delta x}. \tag{4.5}$$

Similarly, as the parameter $\epsilon \to 0$, the other macroscopic interface fluxes will go to

$$\begin{aligned}
\Phi^{n+1}_{g,i+1/2,j} &\to -\frac{4\pi c}{3(\sigma^p_g)^{n+1}_{i+1/2,j}}\frac{\phi^{n+1}_{g,i,j}-\phi^{n+1}_{g,i+1,j}}{\Delta x},\\
\Psi^{n+1}_{g,i,j-1/2} &\to -\frac{4\pi c}{3(\sigma^p_g)^{n+1}_{i,j-1/2}}\frac{\phi^{n+1}_{g,i,j}-\phi^{n+1}_{g,i,j-1}}{\Delta y},\\
\Psi^{n+1}_{g,i,j+1/2} &\to -\frac{4\pi c}{3(\sigma^p_g)^{n+1}_{i,j+1/2}}\frac{\phi^{n+1}_{g,i,j}-\phi^{n+1}_{g,i,j+1}}{\Delta y}.
\end{aligned} \tag{4.6}$$

Thirdly, multiplying the integration weight ω_m to equation (3.25) and summing over the angle variable and frequency variable, as the parameter $\epsilon \to 0$, we have

$$\begin{aligned}
\sum_{g=1}^{G}\rho^{n+1}_{g,i,j} = \sum_{g=1}^{G}\Bigg\{ &\rho^{n}_{g,i,j} + \frac{\Delta t}{\Delta x}\left(-\frac{4\pi c}{3(\sigma^p_g)^{n+1}_{i-1/2,j}}\frac{\phi^{n+1}_{g,i,j}-\phi^{n+1}_{g,i-1,j}}{\Delta x} + \frac{4\pi c}{3(\sigma^p_g)^{n+1}_{i+1/2,j}}\frac{\phi^{n+1}_{g,i,j}-\phi^{n+1}_{g,i+1,j}}{\Delta x}\right)\\
&+ \frac{\Delta t}{\Delta y}\left(-\frac{4\pi c}{3(\sigma^p_g)^{n+1}_{i,j-1/2}}\frac{\phi^{n+1}_{g,i,j}-\phi^{n+1}_{g,i,j-1}}{\Delta y} + \frac{4\pi c}{3(\sigma^p_g)^{n+1}_{i,j+1/2}}\frac{\phi^{n+1}_{g,i,j}-\phi^{n+1}_{g,i,j+1}}{\Delta y}\right)\\
&- c\Delta t\sum_{m=1}^{M}\omega_m((\sigma^a_g)^{n+1}_{i,j}I^{n+1}_{i,j,m,g} - (\sigma^e_g)^{n+1}_{i,j}\phi^{n+1}_{g,i,j})/\epsilon^2\Bigg\}.
\end{aligned} \tag{4.7}$$

The combination of the two equations (4.7) and (3.26) gives

$$\begin{aligned}
\sum_{g=1}^{G}\rho^{n+1}_{g,i,j} = \sum_{g=1}^{G}\Bigg\{ &\rho^{n}_{g,i,j} + \frac{\Delta t}{\Delta x}\left(-\frac{4\pi c}{3(\sigma^p_g)^{n+1}_{i-1/2,j}}\frac{\phi^{n+1}_{g,i,j}-\phi^{n+1}_{g,i-1,j}}{\Delta x} + \frac{4\pi c}{3(\sigma^p_g)^{n+1}_{i+1/2,j}}\frac{\phi^{n+1}_{g,i,j}-\phi^{n+1}_{g,i+1,j}}{\Delta x}\right)\\
&+ \frac{\Delta t}{\Delta y}\left(-\frac{4\pi c}{3(\sigma^p_g)^{n+1}_{i,j-1/2}}\frac{\phi^{n+1}_{g,i,j}-\phi^{n+1}_{g,i,j-1}}{\Delta y} + \frac{4\pi c}{3(\sigma^p_g)^{n+1}_{i,j+1/2}}\frac{\phi^{n+1}_{g,i,j}-\phi^{n+1}_{g,i,j+1}}{\Delta y}\right)\Bigg\} - cC_v(T^{n+1}_{i,j} - T^{n}_{i,j}).
\end{aligned} \tag{4.8}$$

Due to the relations (4.4) and (3.4), we get

$$\begin{cases}
\sum_{g=1}^{g=G} 4\pi\phi^{n+1}_{g,i,j} = \int_0^\infty B(\nu, T^{n+1}_{i,j})d\nu = acT^{n+1}_{i,j},\\
\sum_{g=1}^{g=G}\rho^{n+1}_{g,i,j} = \sum_{g=1}^{g=G} 4\pi\phi^{n+1}_{g,i,j} = acT^{n+1}_{i,j}.
\end{cases}$$

As a result, equation (4.8) becomes a standard five points scheme for the diffusion limit equation (2.3). This shows that the current scheme for the frequency-dependent radiative transfer equations (2.1) is an asymptotic preserving (AP) method. □

The usefulness of UGKS is not limited for the recovery of the kinetic and diffusive limiting solutions. Accurate solutions can be obtained in the whole transition regime as well.

5. Numerical tests

This section presents a number of examples to validate the proposed AP scheme for frequency-dependent radiative transfer equations. In the computations, the unit of length is taken to be centimeter (cm), mass unit is gramme (g), time unit is nanosecond (ns), temperature unit is kilo electronvolt (keV), and energy unit is 10^9 Joules (GJ). Under the above units, the speed of light is 29.98 cm/ns, and the radiation constant a is 0.01372 GJ/(cm^3 keV^4). The time step is determined by $\Delta t = CFL * min(\Delta x, \Delta y)/c$. The Courant number CFL takes a value 0.8 in the following numerical tests.

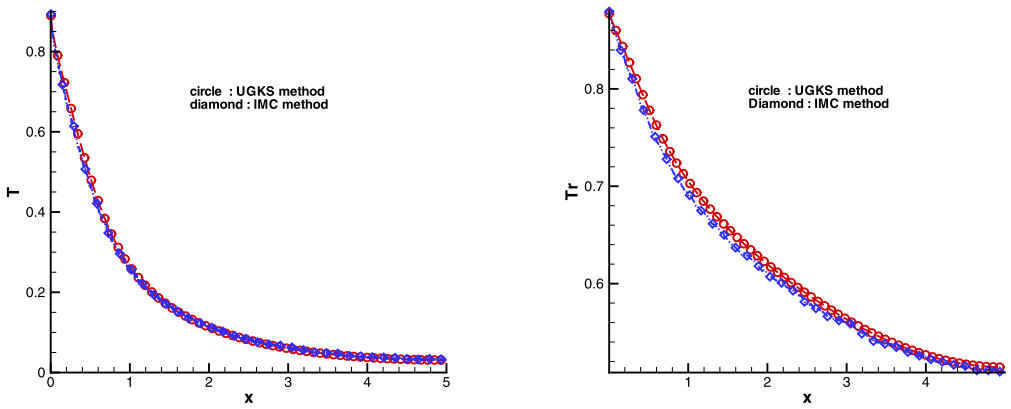

Fig. 2. Results at 1 ns for Case 1 of Example 1 with homogeneous opacity $\sigma_0 = 10$ keV$^{7/2}$/cm.

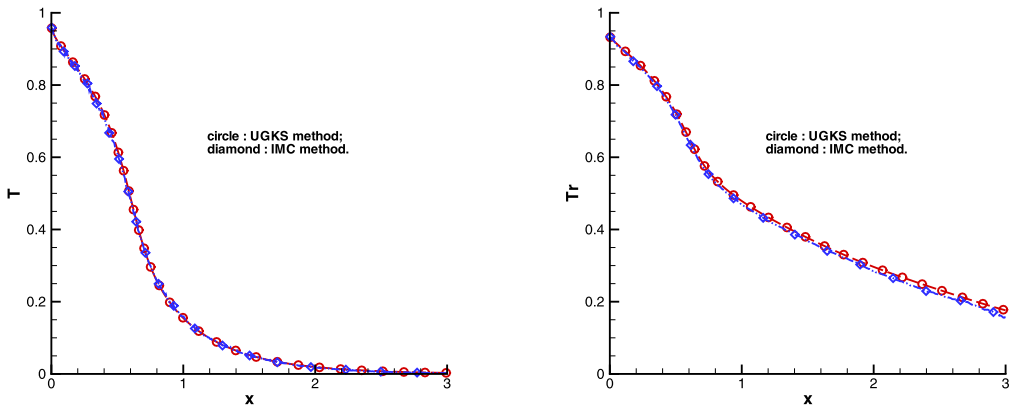

Fig. 3. Results at 1 ns for Case 1 of Example 1 with homogeneous opacity $\sigma_0 = 100$ keV$^{7/2}$/cm.

It should be pointed out that in the following cases the opacity for the reference results of Implicit Monte Carlo (IMC) simulations is evaluated by the Planck averaging method. However, the UGKS method uses simple group integration averaging. In order to compare the computational time of UGKS and IMC, both codes are running in the ThinkPad X250(Intel(R) Core(TM) i7-5600U) machine. The IMC results are obtained by using 1.5 million particles in the computations.

Example 1. (See [6].) In this example, we consider a one-dimensional Cartesian coordinate with a constant heat capacity $C_v = 0.1$ GJ/keV/cm^3 and an opacity of the form

$$\sigma(x, \nu, T) = \frac{\sigma_0(x)}{(h\nu)^3\sqrt{kT}}.$$

The initial material temperature is 10^{-3} keV, and the initial radiation intensity is given by a Planck distribution evaluated at the same temperature. The incident radiation intensity on the left boundary is also given by a Planck distribution, but it is associated with a temperature of 1 keV. A reflective boundary condition is used on the right boundary. This test will cover three cases with different optical opacity specified by σ_0. To represent the frequency-dependent opacity, the UGKS employs 30 frequency groups spaced logarithmically between 10^{-4} keV and 100 keV. The multi-group opacities are evaluated simply by averaging it over each group.

Case 1: Several homogeneous problems are tested in a domain of 5 cm thickness with $\sigma_0 = 10$ keV$^{7/2}$/cm, 100 keV$^{7/2}$/cm, and 1000 keV$^{7/2}$/cm. In all three cases, a uniform spatial mesh is used with cell size $\Delta x = 0.005$ cm and a running time of 1 ns. Figs. 2–4 present the material and radiation temperatures computed from both UGKS and IMC. Note that in Figs. 3 and 4 only the portions with large material temperature variation are shown. The material temperature from UGKS agrees well with the IMC result.

Case 2: In this case, we consider the first heterogeneous problem, which covers a domain of 3 cm thickness divided by an optically thin region 0 cm $< x <$ 2 cm and an optically thick region 2 cm $< x <$ 3 cm, where σ_0 is defined by

$$\sigma_0(x) = \begin{cases} 10 \text{ keV}^{7/2}/\text{cm}, & 0 \text{ cm} < x < 2 \text{ cm}, \\ 1000 \text{ keV}^{7/2}/\text{cm}, & 2 \text{ cm} < x < 3 \text{ cm}. \end{cases}$$

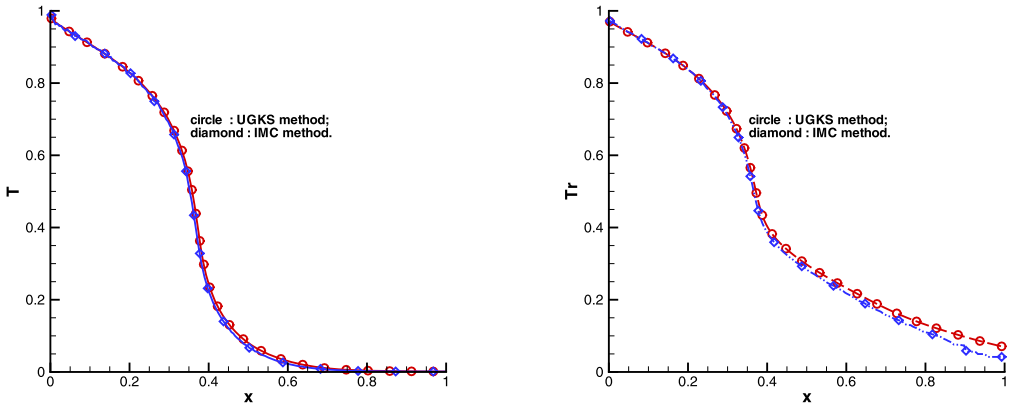

Fig. 4. Results at 1 ns for Case 1 of Example 1 with homogeneous opacity $\sigma_0 = 1000\ \text{keV}^{7/2}/\text{cm}$.

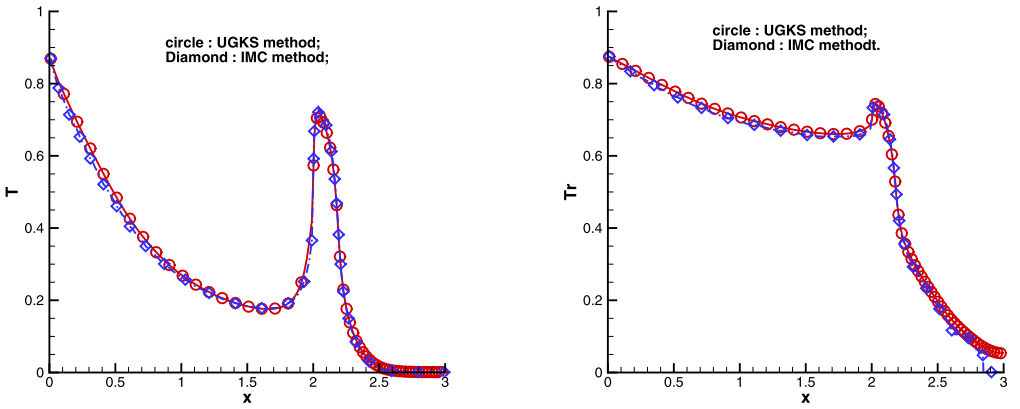

Fig. 5. Results at 1 ns for Case 2 of Example 1 with the first heterogeneous opacities.

In the computation, the cell size is $\Delta x = 0.02$ cm in the optically thin region and $\Delta x = 0.005$ cm in the optically thick region. The simulation runs up to the time of 1 ns. Fig. 5 shows the UGKS and IMC results, where good agreement has been obtained.

Case 3: In this case, we consider the second heterogeneous problem in a domain of 1.5 cm thickness, but with reversed locations for the optically thin and thick regions. Specifically, this domain is composed of an optically thick region in $0\ \text{cm} < x < 0.5$ cm and an optically thin region in $0.5\ \text{cm} < x < 1.5$ cm with σ_0 given by

$$\sigma_0(x) = \begin{cases} 1000\ \text{keV}^{7/2}/\text{cm}, & 0\ \text{cm} < x < 0.5\ \text{cm}, \\ 10\ \text{keV}^{7/2}/\text{cm}, & 0.5\ \text{cm} < x < 1.5\ \text{cm}. \end{cases}$$

A spatial mesh with cell size $\Delta x = 0.02$ cm in the optically thin region and $\Delta x = 0.005$ cm in the optically thick region is used. The simulation runs up to a time of 5 ns. Fig. 6 presents the UGKS and IMC solutions. There are slight differences between these two solutions in the optical thin region.

The computational time of UGKS and IMC for all three cases is shown in Table 1. Generally, the UGKS is much more efficient than IMC method with the same spatial mesh size, especially for the optical thick case.

Example 2 *(Larsen's test problem).* (See [3,15].) For this problem, the frequency variable ν is logarithmically spaced with 50 groups between $h\nu_{min} = 10^{-5}$ keV and $h\nu_{max} = 10$ keV. Group g is defined by $\nu_{g-\frac{1}{2}} \le \nu \le \nu_{g+\frac{1}{2}}$, where

$$\nu_{\frac{1}{2}} = \nu_{min}, \quad \nu_{g+\frac{1}{2}} = \left(\frac{\nu_{max}}{\nu_{min}}\right)^{\frac{1}{50}} \nu_{g-\frac{1}{2}}.$$

The computational domain is divided into three regions with different cell size,

$$\Delta x = \begin{cases} 0.10\ \text{cm}, & 0\ \text{cm} < x < 1\ \text{cm}, \\ 0.02\ \text{cm}, & 1\ \text{cm} < x < 2\ \text{cm}, \\ 0.20\ \text{cm}, & 2\ \text{cm} < x < 4\ \text{cm}. \end{cases}$$

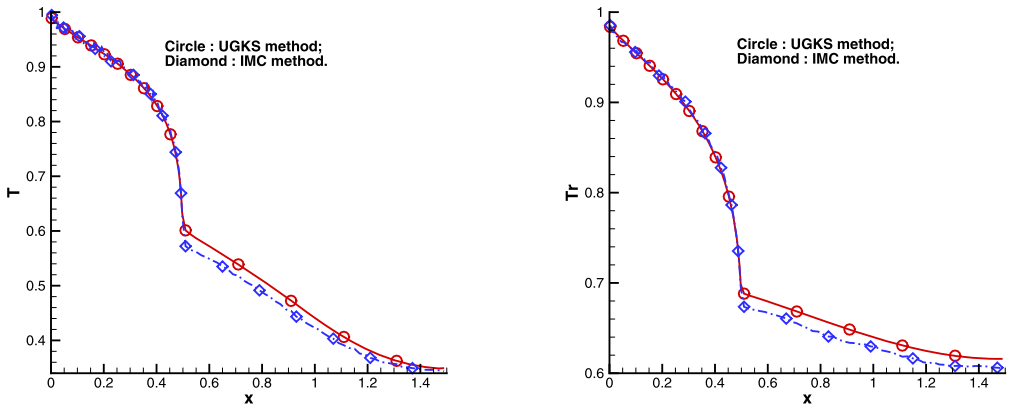

Fig. 6. Results at 5 ns for Case 3 of Example 1 with the second heterogeneous opacities.

Table 1
The computation time of UGKS and IMC for Example 1.

Example 1		UGKS	IMC
Case 1	$\sigma_0 = 10$	21 minutes	96 minutes
	$\sigma_0 = 100$	22 minutes	173 minutes
	$\sigma_0 = 1000$	40 minutes	1344 minutes
Case 2	1st heterogeneous problem	8 minutes	363 minutes
Case 3	2nd heterogeneous problem	34 minutes	5184 minutes

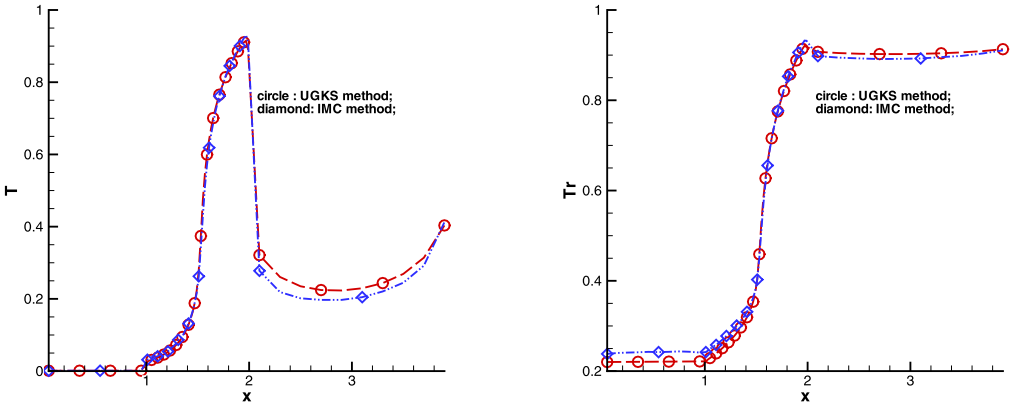

Fig. 7. Results of Larsen's tests (Example 2) at 900 ps.

The opacity models photo-ionization absorption,

$$\sigma(\nu, T, x) = \gamma(x)\frac{1 - e^{-h\nu/kT}}{(h\nu)^3},$$

where

$$\gamma(x) = \begin{cases} 1\ \text{keV}^3/\text{cm}, & 0\ \text{cm} < x < 1\ \text{cm}, \\ 1000\ \text{keV}^3/\text{cm}, & 1\ \text{cm} < x < 2\ \text{cm}, \\ 1\ \text{keV}^3/\text{cm}, & 2\ \text{cm} < x < 4\ \text{cm}. \end{cases}$$

The heat capacity C_v keeps a constant value $5.109 \times 10^{14}\ \text{erg keV}^{-1}\,\text{cm}^{-3}$. The initial material temperature is given by $T(x, 0) = 10^{-3}$ keV, which is in equilibrium with the initial radiation intensity. No radiation enters from the left boundary, but a steady, direction-dependent, 1 keV Planckian distribution of photons enters from the right boundary. The simulation runs up to a time of 900 ps. Fig. 7 shows good agreement between UGKS and IMC solutions in the middle opacity thick region. But small differences appear between these two solutions in both opacity thin regions. The computational cost of UGKS and IMC for this case is given in Table 2.

Table 2
The computation time of UGKS and IMC for Example 2.

UGKS	IMC
2 minutes	63 minutes

6. Conclusion

To numerically simulate multiple frequency radiative transfer in different regimes is difficult for discrete ordinate method (DOM). In this paper we extend the unified gas kinetic scheme from the gray radiative transfer equations to the frequency-dependent radiative transfer system. The key point for the success of UGKS is the un-splitting treatment of photon transport and collision with material in the evaluation of a time-dependent radiation intensity at a cell interface for flux construction, where this evolution solution covers different transport regimes. This approach is different from many single scale operator spitting methods, where the transport and collision are numerically treated separately, such as the Monte Carlo method. In order to capture a valid physical solution, the operator splitting method usually requires a time step being less than the particle collision time. The current UGKS captures the radiative diffusion process in the optical thick region, and the ballistic photon transport in the optical thin regime. Between these limits, the UGKS presents a smooth transition with the variation of the ratio between the time step and local photon's collision time. Many numerical examples, which have been previously tested by the Monte Carlo methods, are calculated by the current DOM-type UGKS as well. The UGKS may be the first DOM which has been used for a full comparison with the IMC method, where comparable solutions are obtained. But, the UGKS is much more efficient than IMC, and its solutions don't sensitively depend on the mesh size and time step. The methodology of unified scheme is general and can be used in many other multiple scale transport processes, such as rarefied gas flow, plasma, and neutron transport.

Acknowledgements

The current research was supported by the Science and Technology Development foundation of China Academy of Engineering Physics (2015B0202041, 2015B0202040) and NSFC (11371068) for Sun; by the National Basic Research Program (2014CB745002, 2011CB309705) and NSFC (11229101, 11371065) for Jiang; by Hong Kong Research Grant Council (620813, 16211014), HKUST SBI14SC11, and NSFC-91330203 for Xu; and by the Science and Technology Development foundation of China Academy of Engineering Physics (2012A0102005) for Li.

References

[1] M.L. Adams, NUEN 630: computational methods for particle-transport problems, class notes, Texas A&M University, 2004.
[2] M.L. Admas, P.F. Nowak, Asymptotic analysis of a computational method for time- and frequency-dependent radiative transfer, J. Comput. Phys. 146 (1998) 366–403.
[3] B. Chang, The incorporation of the semi-implicit linear equations into Newton's method to solve radiation transfer equations, J. Comput. Phys. 226 (2007) 852–878.
[4] S.Z. Chen, K. Xu, C.B. Lee, Q.D. Cai, A unified gas kinetic scheme with moving mesh and velocity space adaptation, J. Comput. Phys. 231 (2012) 6643–6664.
[5] S.Z. Chen, K. Xu, A comparative study of an asymptotic preserving scheme and unified gas-kinetic scheme in continuum flow limit, J. Comput. Phys. 288 (2015) 52–65.
[6] J.D. Densmore, K.G. Thompson, T.J. Urbatsch, A hybrid transport-diffusion Monte Carlo method for frequency-dependent radiative-transfer simulations, J. Comput. Phys. 231 (2012) 6924–6934.
[7] N.A. Gentile, Implicit Monte Carlo diffusion – an acceleration method for Monte Carlo time-dependent radiative transfer simulations, J. Comput. Phys. 172 (2001) 543–571.
[8] J.R. Howell, R. Siegel, M.P. Menguc, Thermal Radiation Heat Transfer, fifth ed., Taylor & Francis, 2011.
[9] J.C. Huang, K. Xu, P.B. Yu, A unified gas-kinetic scheme for continuum and rarefied flows II: multi-dimensional cases, Commun. Comput. Phys. 12 (2012) 662–690.
[10] S. Jin, C.D. Levermore, The discrete-ordinate method in diffusive regimes, Transp. Theory Stat. Phys. 20 (1991) 413–439.
[11] S. Jin, C.D. Levermore, Fully discrete numerical transfer in diffusive regimes, Transp. Theory Stat. Phys. 22 (1993) 739–791.
[12] S. Jin, L. Pareschi, G. Toscani, Uniformly accurate diffusive relaxation schemes for multiscale transport equations, SIAM J. Numer. Anal. 38 (2000) 913–936.
[13] A. Klar, An asymptotic-induced scheme for nonstationary transport equations in the diffusive limit, SIAM J. Numer. Anal. 35 (1998) 1073–1094.
[14] A. Klar, C. Schmeiser, Numerical passage from radiative transfer to nonlinear diffusion models, Math. Models Methods Appl. Sci. 11 (2001) 749–767.
[15] E.W. Larsen, A grey transport acceleration method for time-dependent radiative transfer problems, J. Comput. Phys. 78 (1988) 459–480.
[16] A.W. Larsen, J.E. Morel, Asymptotic solutions of numerical transport problems in optically thick, diffusive regimes. II, J. Comput. Phys. 83 (1989) 212–236.
[17] A.W. Larsen, J.E. Morel, W.F. Miller Jr., Asymptotic solutions of numerical transport problems in optically thick, diffusive regimes, J. Comput. Phys. 69 (1987) 283–324.
[18] E.W. Larsen, G.C. Pomraning, V.C. Badham, Asymptotic analysis of radiative transfer problems, J. Quant. Spectrosc. Radiat. Transf. 29 (1983) 285.
[19] C.E. Lee, The discrete S_N approximation to transport theory, LA-2595, 1962.
[20] L. Mieussens, On the asymptotic preserving property of the unified gas kinetic scheme for the diffusion limit of linear kinetic model, J. Comput. Phys. 253 (2013) 138–156.
[21] M.F. Modest, Radiative Heat Transfer, third ed., Academic Press, 2013.

[22] W.J. Sun, S. Jiang, K. Xu, An asymptotic preserving unified gas kinetic scheme for gray radiative transfer equations, J. Comput. Phys. 285 (2015) 265–279.
[23] B. van Leer, Towards the ultimate conservative difference schemes V. A second-order sequel to Godunov's method, J. Comput. Phys. 32 (1979) 101–136.
[24] K. Xu, Direct Modeling for Computational Fluid Dynamics: Construction and Application of Unified Gas Kinetic Schemes, World Scientific, 2015.
[25] K. Xu, Direct modeling for computational fluid dynamics, Acta Mech. Sin. 31 (2015) 303–318.
[26] K. Xu, J.C. Huang, A unified gas-kinetic scheme for continuum and rarefied flows, J. Comput. Phys. 229 (2010) 7747–7764.